Green Composites Reinforced with Hemp Nanocrystals in Plasticized Starch

Xiaodong Cao,[1] Yun Chen,[1,2] Peter R. Chang,[1] Mark Stumborg,[3] Michel A. Huneault[4]

[1]*BioPoducts and Bioprocesses National Science Program, Agriculture and Agri-Food Canada, 107 Science Place, Saskatoon, Saskatchewan S7N 0X2, Canada*
[2]*Research Centre for Medical and Structural Biology, School of Basic Medical Science, Wuhan University, Wuhan 430071, China*
[3]*Semiarid Prairie Agricultural Research Centre, Agriculture and Agri-Food Canada, P.O. Box 1030, Swift Current, Saskatchewan S9H 3X2, Canada*
[4]*Industrial Materials Institute, National Research Council Canada, 75, de Mortagne, Boucherville, Québec J4B 6Y4, Canada*

Received 14 January 2008; accepted 6 March 2008
DOI 10.1002/app.28418
Published online 6 June 2008 in Wiley InterScience (www.interscience.wiley.com).

ABSTRACT: New nanocomposite films were prepared from a mixed suspension of hemp cellulose nanocrystals (HCNs) and thermoplastic starch, or plasticized starch (PS), by the casting and evaporating method. The morphology, thermal behavior, mechanical properties, and water sensitivity of the films were investigated by means of scanning electron microscopy, wide-angle X-ray diffraction, differential scanning calorimetry, tensile testing, contact angle measurements, and water absorption. The results indicate that the cellulose nanocrystals dispersed in the PS matrix homogeneously and resulted in an increase in the glass-transition temperature ascribed to the fact that the flexibility of the starch molecular chains in the starch-rich phase was reduced because of the strong intermolecular interactions between the starch and stiff HCNs. The films exhibited significant increases in the tensile strength and Young's modulus, from 3.9 to 11.5 MPa and from 31.9 to 823.9 MPa, respectively, with increasing HCN content from 0 to 30 wt %. In addition to the improvement in mechanical properties, the incorporation of HCNs into the PS matrix also led to a decrease in the water sensitivity of the final composite materials. Therefore, the HCNs played an important role in improving the mechanical properties and water resistance of the starch-based material. J Appl Polym Sci 109: 3804–3810, 2008

Key words: nanocomposite; reinforcement; film

INTRODUCTION

With an inevitable increase in the price of petroleum and severe environmental pollution caused by nonbiodegradable petroleum-based polymer materials, there is an urgent need to develop environmentally benign materials from renewable resources. The research and development of novel biodegradable materials mitigate growing environmental threats and concern over the costs and uncertainty of the petroleum supply.[1,2] Among the many kinds of renewable polymers, starch is one of the most studied and promising materials for biodegradable plastics because of its ready availability and low cost.[3,4] In past decades, thermoplastic starch, or plasticized starch (PS), has attracted considerable attention and offered an interesting alternative to synthetic polymers when long-term durability is not needed and rapid degradation is desirable.[5,6] However, compared with the conventional synthetic thermoplastics currently in use, biocomposites based on starch still exhibit some disadvantages, especially poor water resistance and mechanical properties.[7]

Hemp (*Cannabis sativa*) is native to central Asia and has been cultivated all over the world for many years. Hemp fibers can be 3–15 ft long, running the length of the plant, and are one of the strongest natural fibers.[8] The most rapidly expanding application for hemp fiber is as a reinforcement in composites.[9,10] Reported materials in blends with hemp fibers have been polypropylene, polyethylene, and polyester.[11,12] However, the tensile strength of hemp fiber is limited because of its complex structure and the unavoidable imperfections of the cell wall, inherent from growth or induced by processing. Essential improvements can be achieved with cellulose nanocrystals (CNs), which are isolated from the natural fibers, because of their high aspect ratio, high bending strength of about 10 GPa, and high Young's modulus of approximately 150 GPa. More recently, there has been an increased application of CNs as the load-bearing constituent in the development of

Correspondence to: P. R. Chang (changp@agr.gc.ca).
Contract grant sponsor: Canadian Biomass Innovation Network (TID 824 project).

new and inexpensive biodegradable materials.[8] Compared with other inorganic reinforcing fillers, CNs also offer many additional advantages, including a wide variety of fillers available throughout the world, low density, low energy consumption in manufacturing, ease of recycling by combustion, high sound attenuation, and comparatively easy processability due to their nonabrasive nature, which allows high filling levels and, in turn, results in significant cost savings.[9–12] Although CNs were first reported by Fengel and Wegner in 1984,[13] the application of CNs from tunicin (an animal cellulose) as a reinforcing phase in a matrix of latex was reported much later.[14] CNs from several sources, such as tunicin,[15,16] chitin,[17] flax,[18] and others[19–23] have been used in the preparation of biodegradable composite materials.

In this study, we prepared CNs from hemp fiber by hydrolysis with concentrated sulfuric acid and then used the resulting CNs to reinforce a PS matrix for the preparation of a nanocomposite material. We prepared the nanocomposites by casting the mixture of aqueous suspensions of CNs and gelatinized starch solution at various weight ratios of CNs and starch. The structure and performance of the nanocomposite films were investigated by field emission scanning electron microscopy (FESEM), wide-angle X-ray diffraction (WAXD), differential scanning calorimetry (DSC), tensile testing, and water sensitivity testing.

EXPERIMENTAL

Materials

Field pea starch, with an average granule size of about 29 μm and composed of 35% amylose and 65% amylopectin, was supplied by Nutri-Pea, Ltd., Canada (Portage la Prairie, Canada). Raw hemp fiber was supplied by Hempline, Inc. (Delaware, Ontario, Canada). The plasticizer, glycerol (99% purity), concentrated sulfuric acid (98%), and sodium hypochlorite solution (available chlorine = 10–13%) were acquired from Sigma-Aldrich Canada, Ltd. (Oakville, Ontario, Canada) and were used as received.

Preparation of the hemp cellulose nanocrystals (HCNs)

Colloidal suspensions of CNs in water were prepared by the acid-catalyzed hydrolysis of the hemp fiber as described by Dong et al.[24] Briefly, the hemp fibers (30 g) were first cut into small fragments and mixed with a sulfuric acid aqueous solution (250 mL, 64 wt %) and stirred vigorously at 45°C for 4 h. Subsequently, the suspension was neutralized with a sodium hydroxide aqueous solution (40 wt %), discolored by sodium hypochlorite solution, and washed by dialysis. The dispersion of HCNs was achieved through a 30-min ultrasonic treatment. The suspension did not sediment or flocculate because of surface sulfate groups created during the sulfuric treatment.[24,25]

Preparation of the PS/HCN nanocomposite films

The fabrication of the PS/HCN nanocomposite films was based on a convenient solution-casting process. Starch, glycerol, CN suspension, and distilled water were mixed together to obtain a nanocomposite solution with a homogeneous dispersion. The glycerol content was fixed at 36 wt % on the basis of the dry starch matrix. Then, this mixture was charged into a bottom flask equipped with a stirrer and heated at 100°C for 30 min for the starch to be gelatinized. After it was cooled to about 70°C, the resulting paste was degassed *in vacuo* to remove the remaining air and cast in a polystyrene square Petri dish; this was followed by drying in a vent oven at 50°C. By changing the content of HCNs over the range 5, 10, 15, 20, 25, and 30 wt %, we prepared a series of PS/HCN nanocomposites films with a thickness of about 0.3 mm and coded them as PS/HCN-5, PS/HCN-10, PS/HCN-15, PS/HCN-20, PS/HCN-25, and PS/HCN-30, respectively, in which the HCN content was expressed on a water-free PS matrix. As a control, a pure PS film without the addition of HCNs was obtained with the same fabrication process. Before the various characterizations, the resulting films were kept in a conditioning desiccator at 43% relative humidity (RH) for 1 week at room temperature to ensure the equilibration of the water content in the films.

Characterizations

Scanning electron microscopy (SEM) measurements were carried out on a field emission scanning electron microscope (Jeol JSM-6700, Jeol, Ltd., Tokyo, Japan). For the morphology of the HCNs, the diluted HCNs suspension was dropped onto a flake of gold-coated wafer, dried at ambient temperature, and then observed by FESEM with an accelerating voltage of 5 kV. In addition, to study the structure of the nanocomposite films, the failure surfaces of the PS/HCN films after tensile testing were coated with platinum and also observed by FESEM with an accelerating voltage of 5 kV.

DSC measurement of the films was carried out on a DSC204 apparatus (Netzsch Co., Selb, Germany) under a nitrogen atmosphere. Each sample conditioned at 43% RH was subjected to a heating/cooling cycle between −100 and 130°C to obtain reproducible glass-transition temperature (T_g) values. In this

case, T_g was taken at the half-variation in the heat capacity of the second run. The heating rate was 10°C/min.

WAXD patterns were recorded on a Bruker AXS X-ray diffraction instrument (Bruker AXS, Inc., Madison, WI) with Cu Kα radiation (λ = 0.154 nm) at 40 kV and 30 mA at a scan rate of 4°/min. The diffraction angle ranged from 4 to 40°.

The tensile strength and elongation at break of the films were measured on a universal testing machine (CMT 6503, Shenzhen SANS Test Machine Co., Ltd., Shenzhen, China) at room temperature with gauge length of 5 cm and a crosshead speed of 10 mm/min. An average value of five replicates for each sample was taken.

The aqueous contact angles were measured on a First Ten Angstroms FTA 100 series contact angle/surface energy analysis system (First Ten Angstroms, Inc., Portsmouth, VA) with deionized water as the probe liquid. A water droplet was deposited on the sample surface, and the droplet shape was recorded. A charged coupling device video camera and image analysis software were used to determine the contact angle evolution. The results are the average values of quadruplicate measurements.

The kinetics of water absorption was determined for all composites. The samples used were thin rectangular strips with dimensions of 50 × 10 × 0.3 mm^3. The samples were dried at 80°C *in vacuo* overnight and kept at 0% RH (P_2O_5) for 1 week. After weighing, they were conditioned at room temperature in a desiccator of 98% RH ($CuSO_4 \cdot 5H_2O$ saturated solution). The conditioning of samples in a high-moisture atmosphere was preferred to the classical technique of immersion in water because starch is very sensitive to water and can partially dissolve after a long exposure to water.[26] The samples were removed at specific intervals and were weighed until the equilibrium state was reached. The water uptake (WU) of the samples was calculated as follows:

$$\mathrm{WU}(\%) = \frac{W_t - W_0}{W_0} \times 100 \quad (1)$$

where W_0 and W_t were the weights of the sample before exposure to 98% RH and after t h of exposure to 98% RH, respectively. An average value of three replicates for each sample was taken.

RESULTS AND DISCUSSION

Morphology of the HCNs and PS/HCN nanocomposites

The FESEM image of a dilute suspension of the HCNs is shown in Figure 1. The HCNs were very clearly identified from the background although they were not dispersed individually because of the strong interactions among the nanocrystals themselves. It was difficult to estimate the length of the nanocrystals because of their aggregations, but the width of the HCNs was measured to be 30 ± 10 nm. The results of FESEM indicate that the CNs were successfully prepared from hemp by acid hydrolysis.

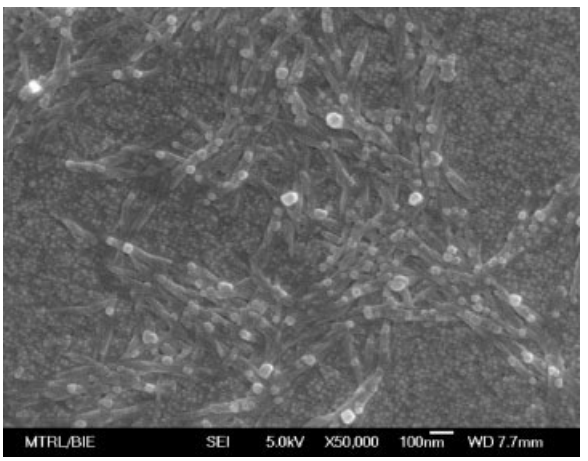

Figure 1 FESEM image of the HCNs dried on gold-coated wafers.

An examination of the fractured surfaces after the tensile testing of the PS/HCN nanocomposites was also carried out with FESEM. Figure 2 shows the images of the PS matrix and nanocomposites filled with 0, 10, 20, and 30 wt % of HCNs, respectively. Compared with the PS film, the morphology of the HCNs in the PS matrix could be easily identified. The HCNs appeared as white dots, whose concentration on the fracture surface of the nanocomposites increased with an increase of the filler loading. Furthermore, a homogeneous distribution of the HCNs in the PS matrix was observed in all of the nanocomposites, which implied that the strong interactions among HCNs themselves were partly destroyed and a new strong adhesion between fillers and matrix was formed. Improved compatibility between HCNs and starch was ascribed to the chemical similarities in starch and cellulose, nanometric size effect from the HCNs, and hydrogen bonding interactions between the fillers and matrix. Such a uniform distribution of the fillers in the matrix could have played an important role in the improvement of the mechanical performance of the resulting nanocomposite films, as discussed later.

WAXD analysis of the PS/HCN nanocomposites

WAXD of the nanocomposites was studied as a function of the HCN content, and the corresponding diffractograms are shown in Figure 3. For the PS film, a typical C-type crystallinity pattern with peaks at 2θ = 5.6° (characteristic of B-type polymorphs), 17.0° (characteristic of both A- and B-type poly-

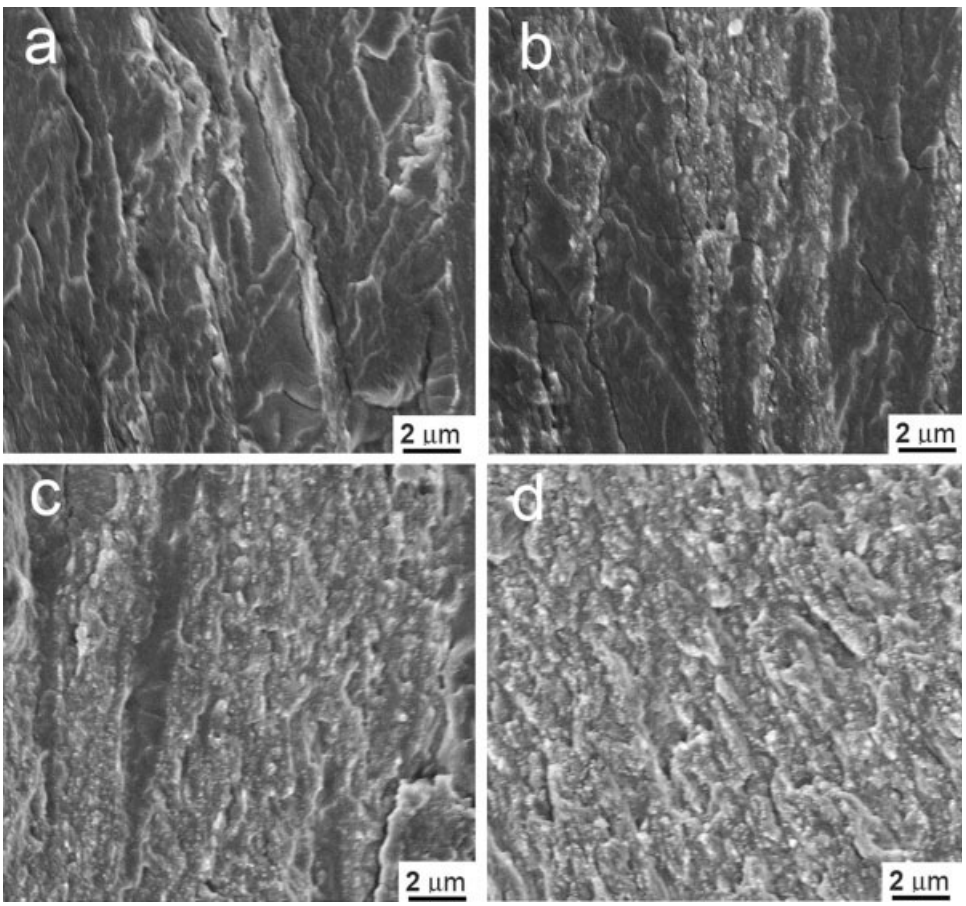

Figure 2 FESEM images of the PS/HCN nanocomposites with different HCN contents: (a) 0, (b) 10, (c) 20, and (d) 30 wt % (scale bar = 2.0 μm).

morphs), and 20.1 and 22.5° (characteristic of B-type polymorphs) were observed clearly.[27] The crystalline structure resulted from the spontaneous recrystallization or retrogradation of starch molecules after gelatinization. This phenomenon has frequently been detected in food and thermoplastic materials based on starch.[28] With an increase in HCNs in the starch matrix, some diffraction peaks appeared in the diffractograms. When the HCN content was increased to more than 15 wt %, three well-defined peaks at 2θ = 14.7, 16.5, and 22.7° were observed. These diffraction peaks were observed in the 100 wt % HCN pattern at the same angles also, which indicated that these diffraction peaks in the nanocomposite materials were attributable to the HCN component. Meanwhile, this result also provides evidence that the original crystalline structure of cellulose remained in the nanocomposite. Although the diffraction peak intensity of the starch and cellulose in the nanocomposite changed with the composition ratio, no evidence of any new peak or peak shift in the diffraction angles was observed. Therefore, we concluded that

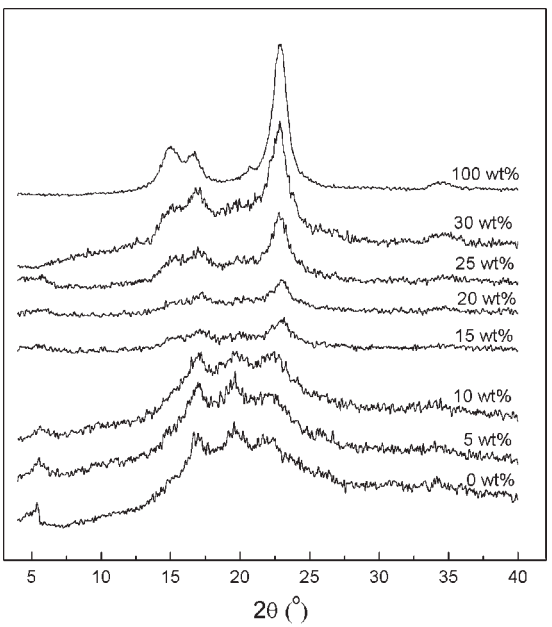

Figure 3 WAXD patterns of the PS/HCN nanocomposites. The HCN contents are indicated in the figure.

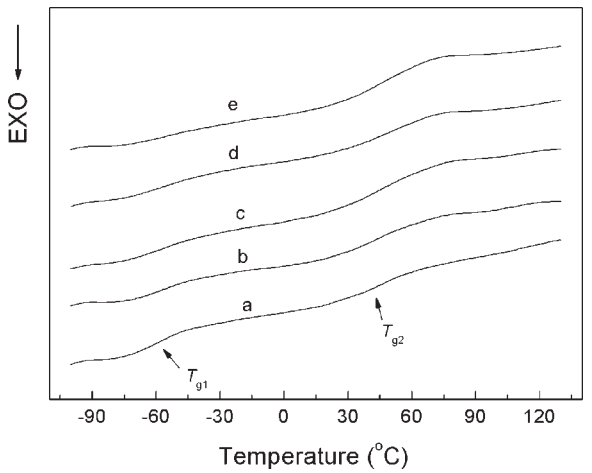

Figure 4 DSC thermograms of the PS and PS/HCN nanocomposites with different HCN contents: (a) 0, (b) 5, (c) 10, (d) 20, and (e) 30 wt %.

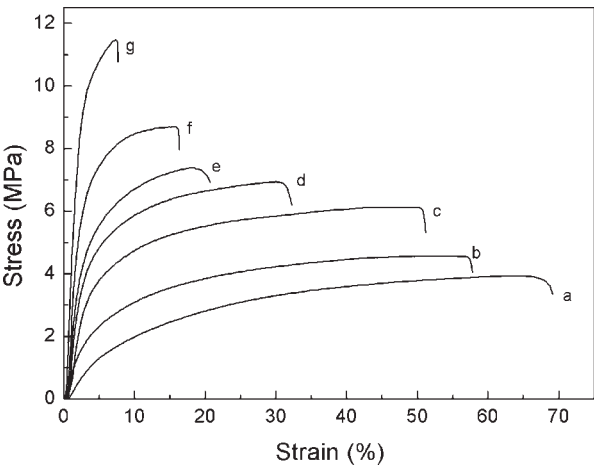

Figure 5 Stress–strain curves of the PS/HCN nanocomposite films with different HCN contents: (a) 0, (b) 5, (c) 10, (d) 15, (e) 20, (f) 25, and (g) 30 wt %.

the diffractograms of the nanocomposites were only superimpositions of the diffractograms of the two components.

Thermal analysis

To further understand the structure and interaction between the two components, DSC studies of the unfilled and filled composites were performed. Figure 4 shows the DSC thermograms in the temperature range −100 to 130°C of the PS/HCN nanocomposites conditioned at 43% RH. All samples displayed two distinct specific heat increments, which corresponded to the T_g of the PS matrix. The data of T_g for the corresponding PS/HCN nanocomposites are also collected in Table I. As we know, the PS plasticized by glycerol existed as a complex heterogeneous system composed of glycerol-rich domains dispersed in a starch-rich continuous phase, and each phase should have exhibited its own T_g.[26,29] Therefore, the transitions located in the temperature range from −80 to −50°C and from 30 to 60°C were associated with the glass transitions of the glycerol-rich phase and starch-rich phase, respectively. With increasing HCN fillers from 0 to 30 wt %, no obvious change in the value of the first T_g at low temperature for the glycerol-rich phase was observed. However, the second T_g for the starch-rich phase shifted to a higher temperature from 43.3 to 48.7°C. The increase in the second T_g dependence on the content of HCNs might have been due to the occurrence of intermolecular interactions between the starch and stiff HCNs, which restricted the mobility of the amorphous starch chains in contact with the HCN surface.

TABLE I
DSC Data of the PS and PS/HCN Nanocomposites

Sample	$T_{g1,\ mid}$ (°C)	ΔC_p (J g^{-1} K^{-1})	$T_{g2,\ mid}$ (°C)	ΔC_p (J g^{-1} K^{-1})
PS	−58.3	0.375	43.3	0.419
PS/HCN-5	−58.1	0.369	44.3	0.405
PS/HCN-10	−57.6	0.354	45.4	0.463
PS/HCN-20	−56.8	0.293	46.4	0.497
PS/HCN-25	−58.6	0.258	48.7	0.467

Tg1, mid and Tg2, mid: The temperatures at the midpoint of the glass transition for starch component in glycerol-rich and in glycerol-poor phase, respectively, as shown in Figure 4; delta Cp: The change in specific heat capacity measured by DSC.

Mechanical properties

The mechanical properties of the unfilled PS films and the nanocomposite films reinforced with various contents of HCNs were investigated by tensile testing at room temperature. The typical stress–strain curves of the PS and its HCN nanocomposites are shown in Figure 5. Clearly, two characteristic regions of deformation behavior were observed. At low strains (< 10%), the stress increased rapidly with increasing strain. At higher strains, the stress regularly increased with the strain up to the break of the films. No evidence of a necking phenomenon at the stress–strain curves confirmed that good dispersion of the HCNs in the matrix and the homogeneous morphology of the nanocomposites, as shown in the FESEM images.

The tensile strength, Young's modulus, and elongation at break were determined from the curves, and the data are presented in Table II. From the results, we observed that the HCN content had a profound effect on the mechanical properties of the films. The tensile strength increased from 3.9 to

TABLE II
Mechanical Properties of the PS and PS/HCN Nanocomposites as Obtained from the Tensile Tests: Tensile Strength (σ), Young's Modulus (*E*), and Elongation at Break (ε_B)

Sample	σ (MPa)	*E* (MPa)	ε_B (%)
PS	3.9 ± 0.3	31.9 ± 5.1	68.2 ± 3.1
PS/HCN-5	4.5 ± 0.2	34.5 ± 4.3	57.3 ± 2.4
PS/HCN-10	6.1 ± 0.5	112.1 ± 13.6	50.4 ± 2.8
PS/HCN-15	6.9 ± 0.4	169.4 ± 10.6	31.2 ± 2.5
PS/HCN-20	7.4 ± 0.7	243.0 ± 30.2	20.3 ± 3.2
PS/HCN-25	8.7 ± 0.4	395.2 ± 15.7	16.4 ± 1.8
PS/HCN-30	11.5 ± 1.3	823.9 ± 25.4	7.5 ± 0.8

11.5 MPa and Young's modulus increased significantly from 31.9 to 823.9 MPa with increasing filler content from 0 to 30 wt %. This can probably be explained by the reinforcement effect from the homogeneously dispersed high-performance HCN fillers in the PS matrix and strong hydrogen bonding interaction between the HCNs and PS molecules. Meanwhile, the elongation at break decreased from 68.2 to 7.5%, which indicated that the incorporation of HCNs restricted the motion of the PS matrix in terms of the strong interactions between the fillers and matrix.

Surface properties and water absorption

Figure 6 shows the effect of HCN content on the initial contact angle values for the PS/HCN nanocomposite films at room temperature. The neat PS film had a low initial contact angle of about 39.5°, and the water droplet on the surface was totally absorbed by the film within 1 min as well. This phenomenon demonstrated the hydrophilic and wettable characteristics of the PS matrix. With the incorporation of HCN fillers into the PS matrix, the contact angle of the nanocomposites increased significantly from 39.5 to 66.5°. This behavior corresponded to the highly crystalline hydrophobic characteristics of the cellulose crystals in comparison with starch's hydrophilic properties.

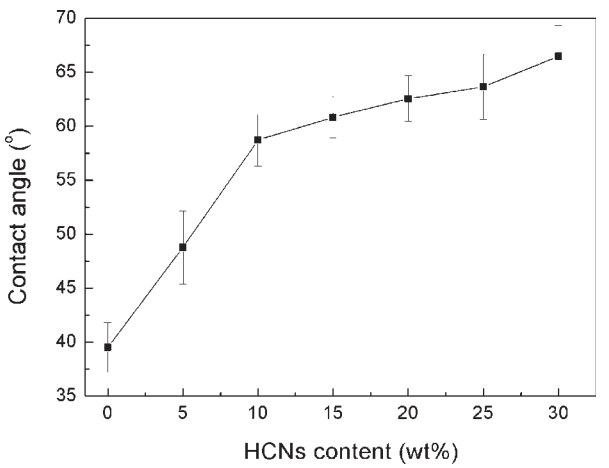

Figure 6 Dependence of the contact angle on the HCN content for the PS/HCN nanocomposite films.

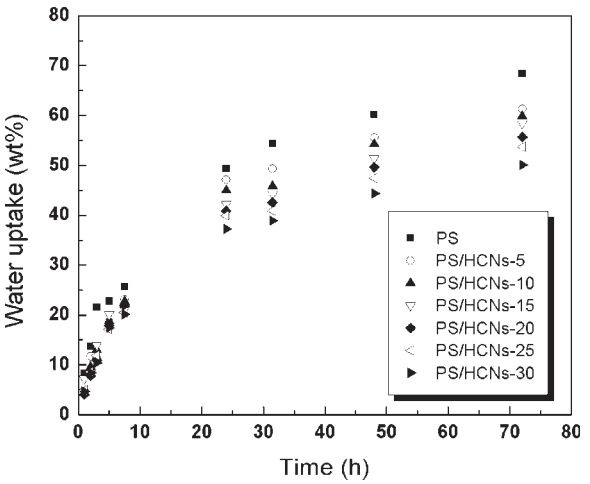

Figure 7 Water uptake during conditioning of 98% RH as a function of time for the PS and PS/HCN films.

The water uptake of the PS and PS/HCN films during conditioning in 98% RH as a function of time is shown in Figure 7. After 3 days, the water uptake of the PS film was around 70 wt %, whereas that of PS/HCN-30 was only around 50 wt %. Therefore, we concluded that the swelling of the material was suppressed in the presence of HCNs within the PS matrix. This phenomenon was ascribed to the presence of strong hydrogen bonding interactions among the fillers themselves and between filler and starch matrix. Meanwhile, the relatively low water sensitivity of the CNs and the low glycerol content in the whole material might have also been responsible for the reduction of the water uptake.

CONCLUSIONS

A suspension of HCNs, with an average width of about 30 ± 10 nm, was prepared from hemp fibers by acid hydrolysis and used to reinforce the PS matrix with contents from 5 to 30 wt % for the preparation of the nanocomposite materials. FESEM images showed that the HCNs fillers dispersed well within the PS matrix and had good adhesion in the interfacial area. The values of T_g ascribed the starch-rich phase increased with an increase of HCN content, which indicated that the HCNs were compatible with the PS matrix and reduced the flexibility of the starch molecular chains. Compared with those of the unfilled PS, the tensile strength and Young's modulus of the nanocomposites increased from 3.9 to 11.5 MPa and from 31.9 to 823.9 MPa, respectively, with an increase of HCN content from 0 to 30 wt %.

Meanwhile, the presence of HCNs also decreased the water sensitivity of the PS/HCN nanocomposites. The performance improvements of the PS/HCN nanocomposites were attributed to the chemical similarities between starch and cellulose, the nanometric size effect of the HCNs, and the hydrogen bonding interactions existing between the fillers and matrix. This study provides a simple method for overcoming poor mechanical properties and moisture sensitivity in PS-based materials through the incorporation of HCNs.

References

1. Mohanty, A. K.; Misra, M.; Drzal, L. T. J Polym Environ 2002, 10, 19.
2. Cakmakli, B.; Hazer, B.; Tekin, I. O.; Kizgut, S.; Koksal, M.; Menceloglu, Y. Macromol Biosci 2004, 4, 649.
3. Choi, E.; Kim, C.; Park, J. J. J Polym Sci Part B: Polym Phys 1999, 37, 2430.
4. Mohanty, A. K.; Misra, M.; Hinrichsen, G. Macromol Mater Eng 2000, 276/277, 1.
5. Suda, K.; Kanlaya, M.; Manit, S. Polymer 2002, 43, 3915.
6. Lepifre, S.; Froment, M.; Cazaux, F.; Houot, S.; Lourdin, D.; Coqueret, X.; Lapierre, C.; Baumberger, S. Biomacromolecules 2004, 5, 1678.
7. Curvelo, A. A. S.; De Carvalho, A. J. F.; Agnelli, J. A. M. Carbohydr Polym 2001, 45, 183.
8. Wang, B.; Sain, M.; Oksman, K. Appl Compos Mater 2007, 14, 89.
9. Masirek, R.; Kulinski, Z.; Chionna, D.; Piorkowska, E.; Pracella, M. J Appl Polym Sci 2007, 105, 255.
10. Behzad, T.; Sain, M. Polym Eng Sci 2007, 47, 977.
11. Wibowo, A. C.; Mohanty, A. K.; Misra, M.; Drzal, L. Ind Eng Chem Res 2004, 43, 4883.
12. Hu, R.; Lim, J. K. J Compos Mater 2007, 41, 1655.
13. Fengel, D.; Wegner, G. de Gruyter: New York, 1984.
14. Favier, F.; Chanzy, H.; Cavaille, J. Y. Macromolecules 1995, 28, 6365.
15. Mathew, A. P.; Dufresne, A. Biomacromolecules 2002, 3, 609.
16. Terech, P.; Chazeau, L.; Cavaille, J. Y. Macromolecules 1999, 32, 1872.
17. Lu, Y.; Weng, L.; Zhang, L. Biomacromolecules 2004, 5, 1046.
18. Cao, X.; Dong, H.; Li, C. M. Biomacromolecules 2007, 8, 899.
19. Sturcova, A.; Davies, G. R.; Eichhorn, S. J. Biomacromolecules 2005, 6, 1055.
20. Podsiadlo, P.; Choi, S.; Shim, B.; Lee, J.; Cuddihy, M.; Kotov, N. Biomacromolecules 2005, 6, 2914.
21. Azizi Samir, M. A. S.; Alloin, F.; Dufresne, A. Biomacromolecules 2005, 6, 612.
22. Kvien, I.; Sugiyama, J.; Votrubec, M.; Oksman, K. J Mater Sci 2007, 42, 8163.
23. Yu, L.; Petinakis, S.; Dean, K.; Bilyk, A.; Wu, D. Macromol Symp 2007, 249–250, 535.
24. Dong, X. M.; Kimura, T.; Revol, J. F.; Gray, D. G. Langmuir 1996, 12, 2076.
25. Marchessault, R. H.; Morehead, F. F.; Walter, N. M. Nature 1959, 184, 632.
26. Angles, M. N.; Dufresne, A. Macromolecules 2000, 33, 8344.
27. Rindlava, Å.; Hulleman, S. H. D.; Gatenholma, P. Carbohydr Polym 1997, 34, 25.
28. Souza Rosa, R. C. R.; Andrade, C. T. J Appl Polym Sci 2004, 92, 2706.
29. Averous, L.; Boquillon, N. Carbohydr Polym 2004, 56, 111.